Wave-induced Roll Motion beneath an Ice Cover

ARNE MELSOM

Institute of Geophysics, University of Oslo, Oslo, Norway

(Manuscript received 16 October 1990, in final form 2 May 1991)

ABSTRACT

A pair of gravity waves propagating at oblique angles along the sea–ice interface in a viscous, rotating ocean is studied theoretically. The motion is described by a Lagrangian formulation. Two theoretical models of the ice cover are considered. Consequences on wave attenuation from these descriptions of the ice are discussed, and the results are compared with field data from the Bering Sea. By use of a series expansion in wave steepness, the nonlinear wave-induced motion is calculated. The mean motion is computed analytically in the case of a nonrotating ocean and numerically in the more general case of a rotating ocean. The induced current is shown to have an exceptional feature; its existence depends on the presence of friction, whereas its magnitude in all directions is independent of the value of the viscosity coefficient. In particular, the computed vertical current is found to be an order of magnitude larger than that obtained for a free surface. Finally, we discuss the importance of wave-induced currents on the vertical transport of nutrients near the ice edge.

1. Introduction

In the last decade there has been a growing interest in the descriptions and explanations of physical processes that take place in the Arctic seas. The rising concern about problems in this area (e.g., the Barents Sea) is due to the fact that there is a potential for commercial offshore oil drilling in the Arctic. This activity may in turn affect the biosphere of the same environment. In this aspect, the vertical mixing of water masses is of vital importance. Here we will try to formulate a theory that describes mean vertical transports when the ocean is covered with ice.

When waves that are generated in the open ocean hit the ice edge, wave energy is reflected, transmitted and absorbed; see, for example, Wadhams et al. (1986). The transmitted wave will be refracted according to Snell's law, and its amplitude will attenuate according to the physical properties of the water and the ice. In the present paper, we shall only consider the transmitted wave and disregard events that occur at the very ice edge. Waves on the sea–ice interface may also be associated with internal waves in the ocean or with wind blowing over sea ice (Squire 1984).

The region of the ice that is close to the edge is known as the marginal ice zone (MIZ). This zone, which extends 50 km or more into the interior of the ice, has been described in detail by Squire and Moore (1980). It is well known that near the ice edge, there is an abundancy of life in the ocean that is not met with elsewhere in the polar areas. An important intention of this paper is to provide one possible explanation for this phenomenon. The basic idea is that the concentration of nutrients in the biologically active layer is increased through vertical mixing. Several theories for describing such mixing have been advanced. One example is the upwelling produced by the motion of the ice edge under wind action (Røed and O'Brien 1983). Another example is the upwelling near the ice edge generated by discontinuity in the wind stress (Gammelsrød et al. 1975). Weber (1987) showed that mean motion induced by unidirectional waves also possesses a discontinuity at the ice edge, which in turn results in upwelling. Here we will consider the effect of a pair of intersecting monochromatic waves that progress and attenuate beneath the ice. It has previously been demonstrated that such a combination of waves does yield periodic, vertical mean motion in the open sea (Weber 1985). We show here that the effect of ice cover enhances this effect. In addition, we find that the mean flow is substantially modified by the effect of the earth's rotation.

During summer, which is the season of high biological activity, the ice melts and the edge retreats up to ten kilometers daily (in the Barents Sea in July; see, e.g., Lunde 1963). Hence, processes that induce mixing beneath the ice have great impact on life conditions for the habitat near the ice edge. When the ice is melting, one may expect to find a surface layer of light, fresh water on top of heavier water. However, for simplicity, we chose to apply a homogeneous model for the ocean. Of course, stratification will inhibit the vertical circulation. Nevertheless, the assumption of homogeneity will not be a serious restraint on the validity

Corresponding author address: Dr. Arne Melsom, University of Oslo, Institute of Geophysics, P.O. Box 1022, Blindern, 0315 Oslo 3, Norway.

of the present model. A complementary discussion on the subject of homogeneity is included in the last section.

The present investigation amounts to a study of fluid motion in the vicinity of a solid boundary. Hence, there are similarities with roll structures in the planetary boundary layer of the atmosphere. A number of papers have been written on this subject [see the review article by Brown (1980)]. These models are chiefly concerned with the stability of a current profile where waves enter the problem as undulating perturbations of a parallel basic flow. However, in the ocean, waves constitute the dominant contribution to the velocity field, exceeding the geostrophic current by an order of magnitude. Thus, the secondary wave-induced motion and the geostrophic current are of comparable magnitude in the ocean, making conditions qualitatively different from those of the atmosphere.

2. Mathematical formulation

We consider an ocean of infinite depth without horizontal bounds rotating about the vertical z axis. The angular velocity of rotation is $f/2$, where f is the Coriolis parameter. The ocean is partly covered with ice of thickness h_0. Furthermore, we assume that the ocean water is viscous and of constant density ρ_0. The coefficient of kinematic viscosity, ν, is also taken to be constant. The motion is described in a right-handed coordinate system where the x, y axes are situated at the undisturbed ice/ocean boundary at the ice edge, such that ice cover is associated with $x \geqslant 0$.

The motion is described by a Lagrangian formulation. Let a fluid particle (a, b, c) have coordinates (x, y, z). We may then write the equations of momentum and continuity:

$$\left.\begin{aligned} x_{tt} - fy_t &= -\frac{1}{\rho_0}\frac{\partial(p, y, z)}{\partial(a, b, c)} + \nu\nabla^2 x_t \\ y_{tt} + fx_t &= -\frac{1}{\rho_0}\frac{\partial(x, p, z)}{\partial(a, b, c)} + \nu\nabla^2 y_t \\ z_{tt} + g &= -\frac{1}{\rho_0}\frac{\partial(x, y, p)}{\partial(a, b, c)} + \nu\nabla^2 z_t \end{aligned}\right\} \quad (2.1)$$

$$\frac{\partial(x, y, z)}{\partial(a, b, c)} = 1, \quad (2.2)$$

where p is the pressure and g is the acceleration due to gravity. Subscripts denote partial differentiation, and $\partial/\partial(a, b, c)$ is the Jacobian. The explicit form of the Laplacian ∇^2 in Lagrangian coordinates is given by Pierson (1962).

This paper considers drift currents due to the interaction of surface gravity waves beneath an ice cover. The identification parameters of a fluid particle correspond to its equilibrium position. That the individual particles actually orbit this position does not affect the second-order mass transport solution (Weber 1983).

We write the position x, y, z and the pressure p as a series expansion (Pierson 1962):

$$\left.\begin{aligned} x &= a + \epsilon x^{(1)} + \epsilon^2 x^{(2)} + \cdots \\ y &= b + \epsilon y^{(1)} + \epsilon^2 y^{(2)} + \cdots \\ z &= c + \epsilon z^{(1)} + \epsilon^2 z^{(2)} + \cdots \\ p &= -\rho g c + \epsilon p^{(1)} + \epsilon^2 p^{(2)} + \cdots \end{aligned}\right\} . \quad (2.3)$$

Here ϵ is an ordering parameter proportional to the amplitude of the surface wave.

As stated in the Introduction, we consider waves with finite crest length. Such waves may occur when waves intersect. In the present analysis, we consider the simplest case; i.e., two monochromatic waves with the same amplitude ζ_0, and wave vectors

$$\left.\begin{aligned} \kappa_1 &= (k, l) \\ \kappa_2 &= (k, -l) \end{aligned}\right\} . \quad (2.4)$$

Here k and l are the wavenumbers in the x and y directions, respectively. This makes the x axis the main propagation direction.

The overall wavenumber is $\kappa = (k^2 + l^2)^{1/2}$, and the corresponding wavelength λ is defined by $\lambda = 2\pi/\kappa$. The crest length $2\pi/l = \lambda\kappa/l$ is always greater than the wavelength. We assume that each of the monochromatic waves causes the ice edge to oscillate with frequency σ and amplitude ζ_0.

For the ordering parameter ϵ we choose

$$\epsilon = \zeta_0 \frac{\sigma}{\kappa} \quad (2.5)$$

(Weber 1985).

Due to viscosity, the waves will attenuate. The damping of the amplitude may be regarded as taking place in either time or space (Lamb 1932). Here the size of the amplitude depends on how far into the ice the waves have propagated. Accordingly, attenuation in space seems to be the natural choice.

3. Linear-wave motion under an ice cover

We restrict ourselves to waves whose frequencies are much larger than the inertial frequency; i.e.,

$$\sigma \gg f. \quad (3.1)$$

The effect of rotation can then be neglected to $O(\epsilon)$ (Pollard 1970).

We take the ice to be a thin elastic plate of thickness h_0 (Tabata 1958). By thin, we mean $\kappa h_0 \ll 1$. Thickening of ice takes place over a distance of several kilometers. Thus, for wavelengths up to several hundred meters, we may assume, to a good approximation, that h_0 is constant. However, it must be realized that, as a model of a real ice cover, an elastic plate constitutes an idealization.

Since the ocean is viscous, we must apply a no-slip condition at the sea–ice interface. This means that at

$c = 0$ there will be no horizontal displacement to $O(\epsilon)$. Furthermore, we require the wave motion to vanish as $c \to -\infty$. To $O(\epsilon)$, the displacement and pressure then become

$$\left.\begin{aligned}
x^{(1)} &= \frac{k}{\sigma}[(e^{\kappa c} - e^{mc})e^{ik\xi} + (e^{\kappa c} - e^{m^* c})e^{-ik\xi}]e^{-\alpha a}\cos lb \\
y^{(1)} &= \frac{l}{\sigma}[i(e^{\kappa c} - e^{mc})e^{ik\xi} - i(e^{\kappa c} - e^{m^* c})e^{-ik\xi}]e^{-\alpha a}\sin lb \\
z^{(1)} &= \frac{\kappa}{\sigma}\left[-i\left(e^{\kappa c} - \frac{\kappa}{m}e^{mc}\right)e^{ik\xi} + i\left(e^{\kappa c} - \frac{\kappa}{m^*}e^{m^* c}\right)e^{-ik\xi}\right]e^{-\alpha a}\cos lb \\
\frac{1}{\rho_0}p^{(1)} &= \sigma\left\{i\left[\left(\frac{g\kappa}{\sigma^2} - 1\right)e^{\kappa c} - \frac{g\kappa}{\sigma^2}\frac{\kappa}{m}e^{mc}\right]e^{ik\xi} - i\left[\left(\frac{g\kappa}{\sigma^2} - 1\right)e^{\kappa c} - \frac{g\kappa}{\sigma^2}\frac{\kappa}{m^*}e^{m^* c}\right]e^{-ik\xi}\right\}e^{-\alpha a}\cos lb
\end{aligned}\right\}. \quad (3.2)$$

Here we have defined $\xi = a - \sigma t/k$ and also the parameters m and γ by

$$m = (1 - i)\left(\frac{\sigma}{2\nu}\right)^{1/2} \equiv (1 - i)\gamma. \quad (3.3)$$

An asterisk denotes complex conjugate. We note that m is inversely proportional to the thickness of the viscous sublayer. The ordering parameter is given by (2.5), and we have assumed that

$$\frac{\kappa}{\gamma} \ll 1. \quad (3.4)$$

For the particular case $l = 0$, (3.2) reduces to the solution given by Weber (1987).

When a wave progresses under an ice cover, the ice takes on the shape of the wave. In wave motion, the oscillatory compressive stress is much smaller than the flexural stress. The mean compressive stress is also neglected. To $O(\epsilon)$, the boundary condition at the sea–ice interface can be written (Liu and Mollo-Christensen 1988):

$$\left[D\nabla_L^4 + \rho_r h_0 \frac{\partial^2}{\partial t^2}\right]z^{(1)} = \frac{1}{\rho_0}p^{(1)} - 2\nu z_{tc}^{(1)}, \quad c = 0. \quad (3.5)$$

Here ρ_r is the relative density of ice to that of seawater. The flexural rigidity D is

$$D = \frac{Eh_0^3}{12(1 - s^2)\rho_0}, \quad (3.6)$$

where E is Young's modulus and s is Poisson's ratio. Furthermore, we have defined

$$\nabla_L^2 = \frac{\partial^2}{\partial b^2} + \frac{\partial^2}{\partial c^2}. \quad (3.7)$$

4. Dispersion and attenuation

In a theory that considers the dynamics of the ice–sea system, one must describe the mechanical behavior of the ice. If the waves are much longer than the ice floes, the ice may be described as an inelastic, inextensible soup, especially when brash ice or grease ice occur (Weber 1987). Thus, the ice–sea system is modeled by two fluids of different viscosity sharing a common interface. In the opposite case, when the waves are much shorter than the floes, one may regard the ice cover as a semi-infinite sheet (Wadhams 1973). Furthermore, taking the absolute creep strain in bending the ice to be negligible compared to the elastic strain (Tabata 1958), the ice cover may be modeled as an elastic plate.

By inserting the $O(\epsilon)$ solution (3.2) into (3.5), we find that the dispersion relation and the coefficient of spatial decay are

$$\sigma^2 = g\kappa(1 + \theta) \quad (4.1a)$$

$$\alpha = \frac{\kappa^3}{2k\gamma}\frac{1 + \theta}{1 + 5\theta}, \quad (4.1b)$$

respectively. Here $\theta = D\kappa^4/g$ is a dimensionless parameter that may not be small. For a given frequency, the dispersion relation (4.1a) yields that waves that penetrate the ice edge become longer beneath the ice cover (Wadhams 1973). Accordingly, by Snell's law, a single wavetrain passing the ice edge at an oblique angle is deflected away from the direction normal to the ice edge or the x axis in this case. This means that l/κ increases on penetration.

In fact, the boundary condition derived from Liu and Mollo-Christensen [i.e., (3.5)] has been obtained under the assumption of an elastic ice cover. When the ice is treated as an inextensible layer, the ice cover will respond to motion with inelastic bending, corresponding to $\theta = 0$. Equation (4.1b) then reduces to the result of Weber (1987). It is worth noting that waves that progress beneath an elastic lid do not decay as rapidly as when the cover responds without elasticity. This is because an elastic plate, when perturbed from its equilibrium position, will oscillate by itself. When the ice is thin and the waves are long (i.e., κh_0 very small), θ becomes small. In that case, the attenuation does not depend much on how the ice is modeled.

During the last decade, there have been several attempts to determine the attenuation of wave energy in the MIZ. Wadhams et al. (1987) have calculated the attenuation coefficient from wave spectra. The spectra have been computed from data gathered by wave buoys placed between ice floes at various distances from the ice edge. The data clearly show that the damping rate depends on frequency as should be expected from (4.1). One situation is depicted in Fig. 1. These data have been published by Squire and Moore (1980) and are based on observations from the Bering Sea in March 1979. Horizontal bars indicate intervals of smoothing, and vertical bars show the least-square errors in an attempt to fit the data within each interval with an exponential curve.

The data has been obtained from stations positioned several kilometers apart, with a maximum distance from the edge of 65 km. One may expect that the ice thickness would have increased significantly from the edge to the innermost station. However, Squire and Moore report that all ice floes visited were less than 0.5 m thick. It should also be noted that their data has been processed under the assumption that attenuation is a function of wave period only. Thus, we take the ice thickness to be constant in Fig. 1 and put $h_0 = 0.3$ m.

It is of some interest to compare field data with the suggested theoretical models. The curves in Fig. 1 correspond to damping rates given by (4.1b). Since the motion in the ocean is turbulent, it seems reasonable to apply a larger value for ν than the molecular one. We have put $\nu = 1.5 \times 10^{-4}$ m^2 s^{-1}, $E = 6 \times 10^9$ Pa, $s = 0.3$, $\rho_0 = 1025$ kg m^{-3}, and $k = \kappa$. Curve (1) represents attenuation by an inelastic cover (i.e., $\vartheta = 0$), whereas curve (2) shows damping by an elastic lid. Since there is no way of determining the value of the eddy viscosity coefficient from the available data, it has been chosen to fit the data. As can be seen, the best agreement with the data is achieved when the ice cover is taken to be elastic. Nevertheless, it should be emphasized that the leftmost part of line 2 corresponds to wavelengths of 45–60 m, whereas the size of the individual ice floes in the considered region varied from 10 m to more than 100 m. If the ice were to act as an elastic cover, one would expect that the typical floe diameter should be much larger than the wavelength. It must also be admitted that the elastic effect indicated by Fig. 1 does not show up in all datasets.

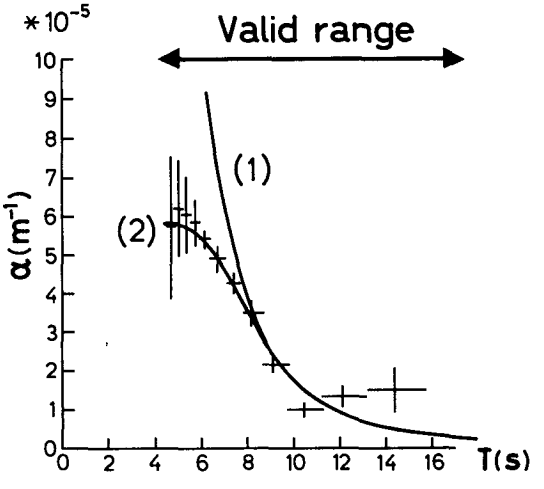

FIG. 1. Wave attenuation rate α versus wave period T. The crosses correspond to observational data from the Bering Sea, March 1979 (Squire and Moore 1980). Labels (1) and (2) correspond to theoretical damping of an inelastic cover and an elastic cover, respectively.

When comparing the data from the Bering Sea with the analytical results (4.1), one should bear in mind that the attenuation rate (4.1b) has been obtained from an idealized situation. In reality, the ocean is covered with separate ice floes, and neither an undivided, semi-infinite sheet, nor a continuous soup of high viscosity. When floes collide, energy is lost due to inelastic deformations. In the present analysis, this effect is incorporated in the parameterization of the coefficient of eddy viscosity, ν.

Of the two options for describing the ice (i.e., inextensible soup and elastic plate), the latter will be adopted here. It should be emphasized that this model of the ice has its deficiencies. In a MIZ environment, the ice floes will be more or less separated. Wave reflection will then not only take place at the ice edge, but within the MIZ as well. Thus, the description of the attenuative processes will be sensitive to the imperfections of the simplified model of the ice cover. However, to develop a model that takes the effects of successive wave reflections into account, is a formidable task and beyond the scope of the present paper.

Finally, it should be stressed that as long as the no-slip condition is imposed at the sea–ice interface, considerations regarding the characteristics of the ice only affect the rate of decay and the dispersion relation, and not the dynamics in the water. Application of a free surface condition at the interface leads to unrealistically high values for the eddy viscosity coefficient, and must, therefore, be discounted (Weber 1987).

5. Wave-drift equations

We introduce mean variables (denoted by an overbar) by averaging over a wave period T:

$$(\overline{x}_t, \overline{y}_t, \overline{z}_t) = \frac{1}{T}\int_t^{t+T} (x_t, y_t, z_t)\,d\tau. \qquad (5.1)$$

For convenience we define dimensionless mean velocity components (u, v, w) and dynamic pressure Π by

$$\left.\begin{aligned}(u, v, w) &= \frac{(\overline{x}_t, \overline{y}_t, \overline{z}_t)}{\zeta_0^2 \sigma k e^{-2\alpha a}} \\ \Pi &= \frac{\bar{p} + \rho_0 g \bar{z}}{\rho_0 \zeta_0^2 \sigma^2 e^{-2\alpha a}}\end{aligned}\right\}. \qquad (5.2)$$

Furthermore, we split up the average velocities u and w to isolate the Stokes drift from the total drift. We also separate the mean inviscid pressure from the total mean pressure, Π. Denoting the differences by variables with carets, we introduce

$$\left.\begin{aligned} \hat{u} &= u - u_s \\ \hat{w} &= w - w_s \\ \hat{\Pi} &= \Pi - \left(1 + \frac{k^2}{\kappa^2}\cos 2lb\right)e^{2\kappa c} \end{aligned}\right\}. \tag{5.3}$$

Here u_s, w_s are the stationary responses from the nonlinear interactions of the inviscid part of the $O(\epsilon)$ solution (3.2), given by

$$\left.\begin{aligned} u_s &= 2\left(1 + \frac{k^2}{\kappa^2}\cos 2lb\right)e^{2\kappa c} \\ w_s &= \frac{\alpha}{\kappa}u_s \end{aligned}\right\}. \tag{5.4}$$

This flow represents a kind of nondivergent Stokes drift. Utilizing the solutions (3.2), the governing equations (2.1) and (2.2) then yield for the nondimensional mean motion to $O(\epsilon^2)$:

$$\hat{u}_t - fv - \nu\nabla_L{}^2\hat{u} + \frac{\sigma}{k}\hat{\Pi}_a = -\sigma\left\{\left[3 + \left(\frac{3k^2 - l^2}{\kappa^2}\right)\cos 2lb\right]e^{2\gamma c} + 4\left[1 + \frac{k^2}{\kappa^2}\cos 2lb\right]\sin\gamma c\, e^{\gamma c}\right\} \tag{5.5}$$

$$v_t + f\hat{u} - \nu\nabla_L{}^2 v + \frac{\sigma}{k}\hat{\Pi}_b = \sigma\frac{l}{k}\left[-\left(\frac{k^2 + 3l^2}{\kappa^2}\right)e^{2\gamma c} + 2\cos\gamma c\, e^{\gamma c}\right]\sin 2lb \tag{5.6}$$

$$\hat{w}_t - \nu\nabla_L{}^2\hat{w} + \frac{\sigma}{k}\hat{\Pi}_c = \sigma\frac{\gamma}{k}\left[1 + \left(\frac{k^2 - l^2}{\kappa^2}\right)\cos 2lb\right] \times (\cos\gamma c - \sin\gamma c)e^{\gamma c} \tag{5.7}$$

$$-2\alpha\hat{u} + v_b + \hat{w}_c = 0. \tag{5.8}$$

We have transformed the second-order momentum equations such that they contain only forcing due to viscosity. The $O(\epsilon^2)$ equations are given by Pierson (1962). However, since they contain some inaccuracies, they are included here in the Appendix in corrected form. Only the leading terms in (κ/γ) have been kept on the right-hand sides of (5.5)–(5.7).

From (4.1b) we observe that α/κ is of $O(\kappa/\gamma)$. Hence, when v and w are of the same order of magnitude as u, we may write (5.8) as

$$v_b + \hat{w}_c = 0. \tag{5.9}$$

The fact that $2\alpha|u| \ll |v_b|, |w_c|$ will be verified a posteriori.

A dimensionless streamfunction ψ is then introduced by writing

$$\left.\begin{aligned} v &= -k^{-1}\psi_c \\ \hat{w} &= k^{-1}\psi_b \end{aligned}\right\}. \tag{5.10}$$

The pressure may be eliminated between (5.6) and (5.7). Thus, we derive an equation for the mean vorticity in the plane perpendicular to the wave propagation direction:

$$\nabla_L{}^2\psi_t - \nu\nabla_L{}^4\psi = Fk\hat{u}_c + 2\sigma l\gamma\left[\left(\frac{k^2 + 3l^2}{\kappa^2}\right)e^{2\gamma c} - 2\frac{l^2}{\kappa^2}(\cos\gamma c - \sin\gamma c)e^{\gamma c}\right]\sin 2lb. \tag{5.11}$$

To $O(\epsilon^2)$, the averaged no-slip condition in the tangential direction at the sea–ice interface becomes

$$\left.\begin{aligned} u &= -\frac{\epsilon^2}{\zeta_0{}^2\sigma k e^{-2\alpha a}}\overline{z_t^{(1)} z_a^{(1)}} = 1 + \cos 2lb \\ \psi_c &= \frac{\epsilon^2}{\zeta_0{}^2\sigma e^{-2\alpha a}}\overline{z_t^{(1)} z_b^{(1)}} = 0 \end{aligned}\right\}, \quad c = 0. \tag{5.12}$$

On average, the ice cover is horizontal and $w\,(c = 0) = 0$. We choose $\psi = 0$ at the origin and obtain

$$\psi\,(c = 0) = 0. \tag{5.13}$$

The drift motion is assumed to vanish at large distance from the surface; that is,

$$u, \psi_c, \psi_b \to 0, \quad c \to -\infty. \tag{5.14}$$

Since the wave motion does not start from a state of rest, there is no unique way of determining the initial condition for the mean drift current. Due to this, we are free to choose an initial condition that satisfies the boundary condition (5.12) at the sea–ice interface. We take

$$\left.\begin{aligned} u\,(t = 0) &= (1 + \cos 2lb)e^{2\kappa c} \\ \psi\,(t = 0) &= 0 \end{aligned}\right\}. \tag{5.15}$$

6. Drift solutions in a nonrotating fluid

When we disregard the earth's rotation, that is, take $f = 0$, the drift currents can be computed analytically. By utilizing the boundary conditions (5.12)–(5.14) and the initial condition (5.15), the streamfunction is obtained from (5.11). By applying Laplace transforms, we finally obtain

$$\psi = \sin 2lb\left\{2\frac{l^2}{\kappa^2}\frac{l}{\gamma}(\sin\gamma c - \cos\gamma c)e^{\gamma c} + \frac{k^2+3l^2}{4\kappa^2}\left[2lce^{2lc} - \frac{l}{\gamma}e^{2\gamma c}\right] + \frac{k^2+3l^2}{\kappa^2}\frac{l}{2\pi\gamma}\right.$$
$$\left.\times\int_0^\infty\left[e^{2lc} - \cos 2\gamma c\xi - \frac{l}{\gamma\xi}\sin 2\gamma c\xi\right]\frac{\xi^2 e^{-2\sigma t\xi^2}d\xi}{[\xi^2 + l^2/\gamma^2]^2(\xi^2+1)} + \frac{l^2}{\kappa^2}\frac{2l}{\pi\gamma}\int_0^\infty\frac{\cos 2\gamma c\xi e^{-2\sigma t\xi^2}d\xi}{\xi^4 + 1/4}\right\}. \quad (6.1)$$

The nondimensional velocity components in the crosswave plane (i.e., the yz plane) then become

$$v = \frac{l}{k}\sin 2lb\left\{\frac{1}{2}\frac{k^2+3l^2}{\kappa^2}[e^{2\gamma c} - (1+2lc)e^{2lc}] - 4\frac{l^2}{\kappa^2}\sin\gamma c e^{\gamma c} - \frac{k^2+3l^2}{\pi\kappa^2}\frac{l}{\gamma}\right.$$
$$\left.\times\int_0^\infty\left[e^{2lc} + \frac{\gamma\xi}{l}\sin 2\gamma c\xi - \cos 2\gamma c\xi\right]\frac{\xi^2 e^{-2\sigma t\xi^2}d\xi}{[\xi^2 + l^2/\gamma^2]^2(\xi^2+1)} + \frac{l^2}{\kappa^2}\frac{4}{\pi}\int_0^\infty\frac{\xi\sin 2\gamma c\xi e^{-2\sigma t\xi^2}d\xi}{\xi^4 + 1/4}\right\} \quad (6.2)$$

$$w = \frac{l}{k}\frac{k^2+3l^2}{\kappa^2}\cos 2lb\left\{lce^{2lc} + \frac{l}{\pi\gamma}\int_0^\infty\left[e^{2lc} - \cos 2\gamma c\xi - \frac{l}{\gamma\xi}\sin 2\gamma c\xi\right]\frac{\xi^2 e^{-2\sigma t\xi^2}d\xi}{[\xi^2 + l^2/\gamma^2]^2(\xi^2+1)}\right\}. \quad (6.3)$$

The streamfunction (6.1) describes roll motion in the yz plane. Thus, the axes of the rolls are aligned along the direction of the wave propagation. The direction of rotation within the rolls is opposite in adjacent cells. This is shown in the conceptual sketch (Fig. 2). For aesthetic reasons, we have put $ly = l\hat{y} + \pi/2$. Then, the x axis is situated at a nodal line.

The nonrotating problem in the x direction, given by (5.5), does not have a steady solution that satisfies the boundary conditions (5.12) and (5.14). It constitutes a diffusion problem with a time-independent internal source of mean momentum. As time increases, the mean velocity will increase without bounds. On a rotating earth, this development will be arrested by the inclusion of the Coriolis force. This problem will be discussed in the next paragraph.

Since the source decays away from the boundary $c = 0$, the appropriate condition is

$$u \text{ bounded as } c \to -\infty. \quad (6.4)$$

It is obvious that $\hat{\Pi}$ will be of order $(\kappa/\gamma)^0$ [e.g., by integration of (5.7)]. Hence, to the lowest order, $\hat{\Pi}_a$ can be neglected in (5.5). We may now calculate the velocity in the direction of wave propagation. With $f = 0$ and $\hat{\Pi}_a = 0$, Eq. (5.5) and the boundary conditions (5.12) and (6.4) yield the induced motion in the direction of wave propagation:

$$u = \left\{e^{2\kappa c} + \frac{3}{2}e^{2\gamma c} - 4\cos\gamma c e^{\gamma c} + \frac{5}{2} + \frac{1}{\pi}\int_0^\infty\left[\frac{8}{4\xi^4+1} - \frac{3}{\xi^2+1}\right]\frac{\sin 2\gamma c\xi}{\xi}e^{-2\sigma t\xi^2}d\xi\right\}$$
$$+ \cos 2lb\left\{\frac{k^2}{\kappa^2}e^{2\kappa c} + \frac{5k^2+3l^2}{2\kappa^2}e^{2lc} + \frac{3k^2-l^2}{2\kappa^2}e^{2\gamma c} - 4\frac{k^2}{\kappa^2}\cos\gamma c e^{\gamma c}\right.$$
$$\left.+ \frac{2}{\pi\kappa^2\gamma^2}\int_0^\infty\left[\frac{4k^2\gamma^2}{1+4\xi^4} + \frac{k^2l^2}{\xi^2+\kappa^2/\gamma^2} - \frac{\gamma^2(3k^2-l^2)}{2(1+\xi^2)}\right]\frac{\xi\sin 2\gamma c\xi}{[\xi^2 + l^2/\gamma^2]}e^{-2\sigma t\xi^2}d\xi\right\}. \quad (6.5)$$

For inviscid wave motion in a nonrotating fluid, the individual particles do not describe exactly closed trajectories, but posses a mean drift of $O(\epsilon^2)$ in the direction of wave propagation (Stokes 1847). When the fluid is viscous, the Lagrangian mean velocity shear near the surface is twice the value of the irrotational shear. This intensification is independent of the value of the coefficient of kinematic viscosity, ν (Longuet-Higgins 1953). At a solid boundary, the inclusion of viscosity implies a no-slip condition. The mean velocity shear in the direction of wave propagation is then increased by an order of magnitude in γ/k in the viscous sublayer. Again, there is an intensification of the velocity that is independent of ν [see (6.5) or Weber 1987]. As can be seen from (6.1), the steady roll motion induced by a pair of intersecting waves under ice exhibits the same remarkable feature throughout the wave zone. Note that this implies a strong vertical current.

Weber (1985) calculated roll motion induced by intersecting waves in the open ocean. Comparing with his results, we find that the velocity in the rolls increases by a factor proportional to γ/κ, i.e., one order of magnitude, when the no-slip condition is imposed. Hence, when compared to an open-ocean situation, there is relatively more energy in the mean motion induced by a pair of waves under ice. At the same time, the rate of attenuation of linear wave motion, α, is also in-

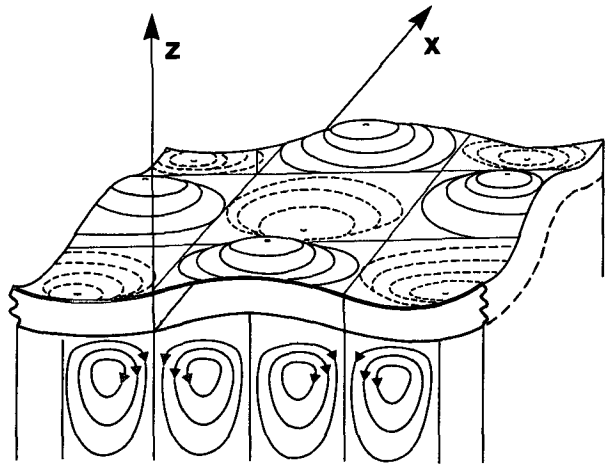

FIG. 2. Sketch of the induced roll motion together with the primary wave field and the displaced ice cover. The waves advance in the direction of the arrow.

creased by one order of magnitude. Accordingly, owing to the no-slip condition, wave energy dissipates much faster under ice than in the open ocean. The ice cover thus provides an effective source of mean, second-order vorticity.

Furthermore, we note that the velocities in all directions are of the same order of magnitude [cf., (6.2), (6.3) and (6.5)]. We have then justified our a priori assumption that led to the introduction of the streamfunction ψ; i.e.,

$$|\hat{u}_a| \ll |v_b|, |\hat{w}_c|. \tag{6.6}$$

The evolution of the rolls is depicted in Fig. 3 for a typical sea state in the marginal ice zone. We have taken $\lambda = 70$ m, $\nu = 10^{-3}$ m^2 s^{-1}, $h_0 = 0.25$ m, $E = 6 \times 10^9$ N m^{-2}, and $s = 0.3$. We have also chosen $\Theta = \tan^{-1}(0.5) = 26.6^0$; Θ being the angle between the waves and the main propagation direction. Isolines for ψ have been drawn with an equidistance $\Delta\psi = 0.02$. Figures 3a,b correspond to $t = 3$ hours and the steady solution, respectively. The dimensional cell width is $\pi/(2l)$, which with the present choice of parameters becomes 40 m.

It is interesting to observe that convergence zones occur at the nodes of the primary wave system analogous to acoustic streaming in Kundt's dust tube. This was also found by Weber (1985) for the free surface case. Furthermore, one may note that for the so-called Langmuir circulation [see the review article by Leibovich (1983)], downwelling zones occur beneath lines of maximum surface velocity. Although for entirely different reasons, this is also the case for the present problem.

7. Effects of rotation

As can be seen from Fig. 3, the rolls develop on a time scale of several hours. Accordingly, the effect of the earth's rotation should be taken into account. This is particularly important in Arctic regions, where the Coriolis parameter has its largest value. The equations to be solved are (5.5) and (5.11). In the present paper, we are primarily interested in the vertical circulation; i.e., the determination of the streamfunction ψ.

In the presence of intersecting waves, u becomes a sinusoidally varying current in the horizontal direction, see (6.5). When this current is shifted toward the direction in which it varies, vertical circulation is induced due to continuity. Indeed, from (5.11), we see that rotation (the shifting mechanism) provides a new source of vorticity through the Coriolis force. This has previously been pointed out by Weber (1985). However, neither qualitative features, nor quantitative estimates of the effect of the Coriolis force on wave induced currents, have hitherto been examined in a Lagrangian framework.

The time-dependent problem for a rotating ocean is solved numerically. We choose a Crank–Nicholson scheme of second-order accuracy. It is then straight-

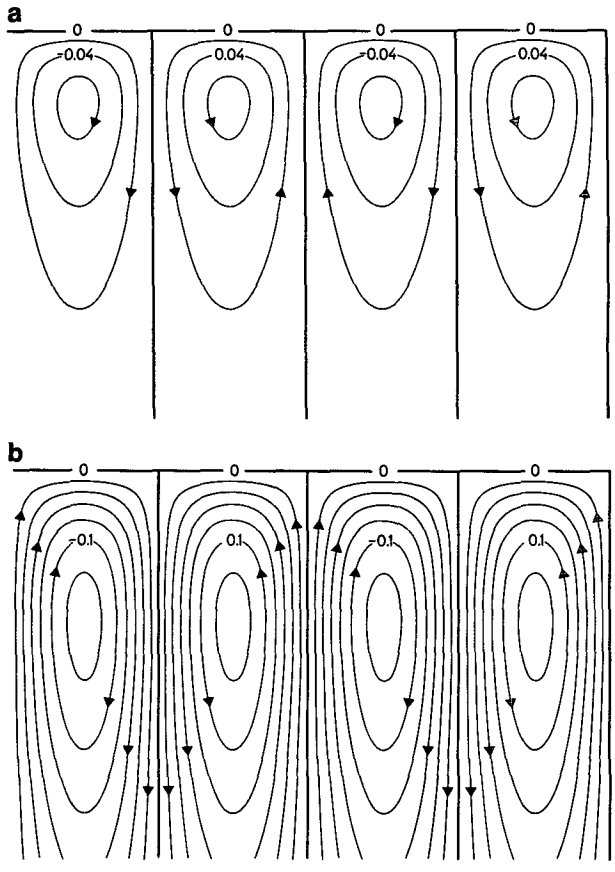

FIG. 3. Streamlines for the dimensionless streamfunction ψ in the plane perpendicular to the crests' propagation direction. Panel (a) corresponds to the situation after 3 h, whereas the steady state is depicted in (b). Here ψ is given by (6.1) and (6.6); see the text for details. With the present choice of parameters, the depth and width of each figure are 35 and 160 m, respectively. The equidistance is $\Delta\psi = 0.02$.

forward to compute the time-dependent solution. The finite difference versions of (5.5) and (5.11) are solved alternately to keep second-order accuracy in time. Here one is faced with the problem that three different length scales have to be resolved. These scales are (i) the Stokes depth $[(2l)^{-1}]$, (ii) the Ekman depth $[(2\nu/f)^{1/2}]$, and (iii) the thickness of the viscous sublayer $[\gamma^{-1}]$. Since $\gamma/l = O(500)$, these scales are very different. In order to test the accuracy, the nonrotating problem was solved numerically. When comparing the analytical solution with the computed results, the error was found to be approximately 5%.

In the computations, we have put $f = 1.4 \times 10^{-4}$ s^{-1}, which corresponds to 74°N. Otherwise, we have chosen the same parameter values as used earlier (see section 6). The solution is depicted in Fig. 4, where Figs. 4a,b again correspond to $t = 3$ hours and the steady solution, respectively. The equidistance between the isolines is now 0.1.

We still find zones of convergence and divergence at the sea–ice interface, but this feature is much less evident than in the hypothetical case of a nonrotating ocean. The water that is not trapped in roll motion now moves toward the right as seen in the direction of wave propagation (the streamfunction is negative except for a narrow region near the interface).

When the numerical scheme has been implemented, it is easy to examine the effect of the somewhat arbitrarily chosen initial condition (5.15). Naturally, the steady solution is independent of the starting condition. To investigate the significance of the initial condition, the problem was solved with $u(t = 0) = 0$. The consequence of this was that the maximum value of the streamfunction was reduced by approximately one-half, one-third, and one-tenth after one, three, and six hours, respectively. Accordingly, a study of the initial value problem is desirable, but such an investigation is beyond the scope of the present paper.

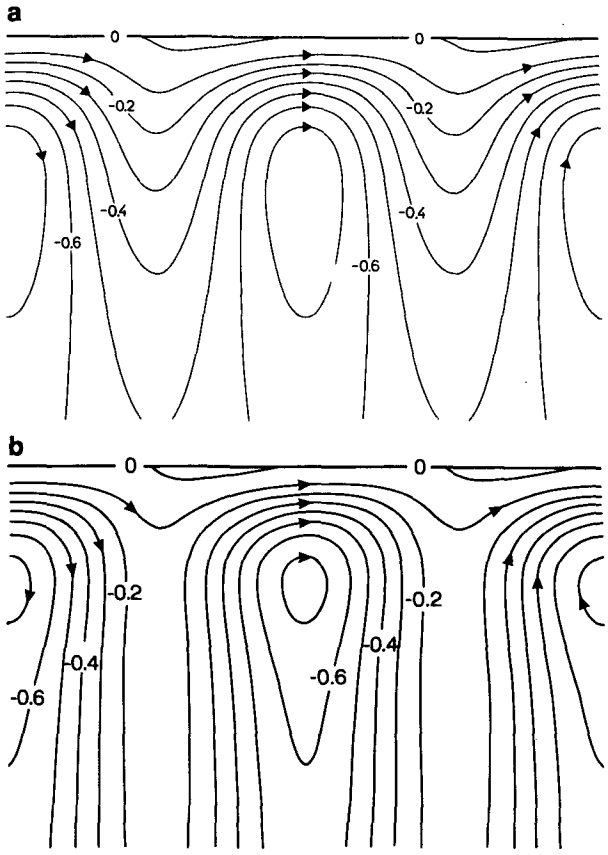

FIG. 4. Same as in Fig. 3, but now for $f = 1.4 \times 10^{-4}$ s^{-1}. The equidistance is now $\Delta\psi = 0.1$.

8. Discussion and conclusions

The present circulation model assumes a homogeneous ocean. In reality, the vertical motion will to some extent depend upon the stratification of the seawater. Hence, the wave-induced roll motion may be somewhat restricted initially. However, this circulation will by itself provide a mixing mechanism and eventually erode the stratification, depressing the pycnocline to the base of the wave zone.

In the vicinity of a solid boundary such as an ice cover, the barotropic tidal current will be modified, and a shear flow will develop. Thus, turbulent mixing will take place in the water beneath the ice. In shallow waters, there is a potential for amplification of tidal motion. Since continental shelves are a dominant feature of the polar oceans, one is led to believe that turbulent mixing may be strong in these regions. Indeed, investigations reveal that in the western Barents Sea, the M_2 tidal current has a characteristic value of 25 cm s^{-1}, and a maximum value of 80 cm s^{-1} (Gjevik et al. 1990). It follows from this discussion that wherever currents are strong relative to the ice, the stratification is expected to be weak even prior to the formation of propagating waves.

Examining datasets from the MIZ, we find that seawater is 1) well mixed in the Bering Sea (winter conditions; Squire and Moore 1980); 2) well mixed above a pycnocline situated at a depth of 25 m or below in the northern Barents Sea (summer conditions; Mosby 1938); and 3) well mixed in the Fram Strait, at least in certain situations (winter conditions; Buckley et al. 1979).

As can be seen from (5.11), there are basically two mechanisms capable of generating roll motion beneath an ice cover. The effect of one of these mechanisms, viscosity, was studied in section 6. The second is the earth's rotation, and the combined effect of viscosity and rotation was examined in section 7. The effect of rotation was found to be dominant. Interaction between viscosity and rotation gives rise to asymmetrical motion. However, due to the dominance of rotation, the asymmetry is very weak. The idea that the effect of the earth's rotation may modify wave-induced roll

motion was first advocated by Woodcock (1944). Still, to the author's knowledge, this has not been established by any mathematically formulated theory prior to the present investigation.

Computations reveal that u, the velocity in the wave propagation direction (i.e., x) possesses a strong shear in the viscous sublayer. The shear develops almost instantly (i.e., within a minute or so), because the interface acts as a vorticity source. This feature of wave-induced currents beneath an ice cover was originally recognized by Weber (1987). If we choose the values of the parameters as earlier, and put $\zeta_0 = 0.5$ m, we find that the maximum wave-induced velocity is approximately 6 cm s^{-1}.

The motivation of the present study has been to examine how wave-induced currents may act as a mixing mechanism beneath ice. When we focus on the mixing of nutrients, the vertical velocity is of special interest.

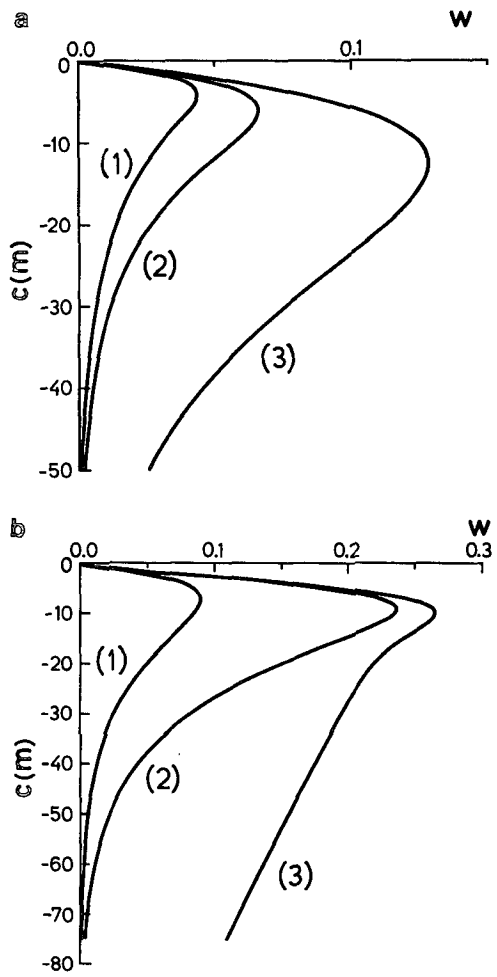

FIG. 5. The maximum dimensionless upward velocity w as a function of depth. Solutions are for (a) a nonrotating and (b) a rotating ocean. Labels (1) and (2) correspond to the vertical current after 1 h and 3 h. The steady solution is labeled by (3). The physical parameters are the same as in Figs. 3 and 4. See the text for details.

In order to assess its effectiveness, the maximum upward mean velocity has been calculated. In Fig. 5, the dimensionless vertical mean velocity, w, is depicted as a function of depth. Labels (1), (2), and (3) correspond to the upward velocity after 1 hour, 3 hours, and the steady situation, respectively. Figure 5a shows the nonrotational solution, whereas Fig. 5b displays the corresponding result when $f = 1.4 \times 10^{-4}$ s^{-1}. For the rest of the parameters the values are as chosen before: $\lambda = 70$ m, $\nu = 10^{-3}$ m^2 s^{-1}, $h_0 = 0.25$ m, $E = 6 \times 10^9$ N m^{-2}, $s = 0.3$, $\Theta = 26.6^0$.

Again, we note the importance of including the earth's rotation. If we choose $\zeta_0 = 0.5$ m, we find that $w = 0.1$ corresponds to a dimensional velocity of 6.75 m h^{-1}. When the effect of rotation is taken into account, the maximum dimensional upward velocity after 3 hours is approximately 18 m h^{-1}. Thus, wave-induced currents provide an effective mechanism for vertical mixing of nutrients.

If the directional dependence of the wave spectrum is ignored (i.e., $l = 0$), the vertical velocity only becomes a fraction of what has been demonstrated here (Weber 1987). Hence, the presence of finite crest-length waves is needed for roll formation. The directional spectrum of a wind-generated sea is symmetric (Longuet-Higgins 1962), justifying the simple model chosen in the present paper.

From Fig. 4 we observe that vertical motion does not extend quite to the sea–ice interface, but stops a few meters underneath. However, near the retreating ice edge in the melting season, sunlight will penetrate the uppermost meters of the ocean. This has been established through measurements of irradiance transmittance by Aas and Berge (1976). Consequently, the mechanism described in this paper is able to transport nutrients vertically into the biologically active layer.

Acknowledgments. This research was partly sponsored by Statoil under Contract T 7333. I am grateful for their support. I would also like to express my gratitude to professor J. E. Weber for the idea that originally initiated the present work. I also wish to thank him for many enlightening discussions and valuable comments on the manuscript.

APPENDIX

The Second-Order Momentum Equations

The governing equations for the second-order motion are

$$x_{tt}^{(2)} - f y_t^{(2)} - \nu \nabla_L^2 x_t^{(2)} + \Pi_a^{(2)} = \frac{1}{\rho} \{ p_a^{(1)} x_a^{(1)} + p_b^{(1)} y_a^{(1)} + p_c^{(1)} z_a^{(1)} \}$$

$$+ g\frac{\partial(y^{(1)}, z^{(1)})}{\partial(a, b)} - 2\nu\{x_a{}^{(1)}x_{taa}^{(1)} + y_b{}^{(1)}x_{tbb}^{(1)} + z_c{}^{(1)}x_{tcc}^{(1)} + (x_b{}^{(1)} + y_a{}^{(1)})x_{tab}^{(1)} + (x_c{}^{(1)} + z_a{}^{(1)})x_{tac}^{(1)} + (y_c{}^{(1)} + z_b{}^{(1)})x_{tbc}^{(1)}\} - \nu\{x_{ta}^{(1)}\nabla_L{}^2x^{(1)} + x_{tb}^{(1)}\nabla_L{}^2y^{(1)} + x_{tc}^{(1)}\nabla_L{}^2z^{(1)}\} \quad \text{(A1)}$$

$$y_{tt}^{(2)} + fx_t^{(2)} - \nu\nabla_L{}^2y_t^{(2)} + \Pi_b{}^{(2)} = \frac{1}{\rho}\{p_a{}^{(1)}x_b{}^{(1)} + p_b{}^{(1)}y_b{}^{(1)} + p_c{}^{(1)}z_b{}^{(1)}\} - g\frac{\partial(x^{(1)}, z^{(1)})}{\partial(a, b)} - 2\nu\{x_a{}^{(1)}y_{taa}^{(1)} + y_b{}^{(1)}y_{tbb}^{(1)} + z_c{}^{(1)}y_{tcc}^{(1)} + (x_b{}^{(1)} + y_a{}^{(1)})y_{tab}^{(1)} + (x_c{}^{(1)} + z_a{}^{(1)})y_{tac}^{(1)} + (y_c{}^{(1)} + z_b{}^{(1)})y_{tbc}^{(1)}\} - \nu\{y_{ta}^{(1)}\nabla_L{}^2x^{(1)} + y_{tb}^{(1)}\nabla_L{}^2y^{(1)} + y_{tc}^{(1)}\nabla_L{}^2z^{(1)}\} \quad \text{(A2)}$$

$$z_{tt}^{(2)} - \nu\nabla_L z_t^{(2)} + \Pi_c{}^{(2)} = \frac{1}{\rho}\{p_a{}^{(1)}x_c{}^{(1)} + p_b{}^{(1)}y_c{}^{(1)} + p_c{}^{(1)}z_c{}^{(1)}\} + g(x_c{}^{(1)}z_a{}^{(1)} + y_c{}^{(1)}z_b{}^{(1)} + z_c{}^{(1)2}) - 2\nu\{x_a{}^{(1)}z_{taa}^{(1)} + y_b{}^{(1)}z_{tbb}^{(1)} + z_c{}^{(1)}z_{tcc}^{(1)} + (x_b{}^{(1)} + y_a{}^{(1)})z_{tab}^{(1)} + (x_c{}^{(1)} + z_a{}^{(1)})z_{tac}^{(1)} + (y_c{}^{(1)} + z_b{}^{(1)})z_{tbc}^{(1)}\} - \nu\{z_{ta}^{(1)}\nabla_L{}^2x^{(1)} + z_{tb}^{(1)}\nabla_L{}^2y^{(1)} + z_{tc}^{(1)}\nabla_L{}^2z^{(1)}\} \quad \text{(A3)}$$

Here

$$\Pi^{(2)} = \frac{1}{\rho}p^{(2)} + gz^{(2)}.$$

The second-order equation of continuity is

$$x_a{}^{(2)} + y_b{}^{(2)} + z_c{}^{(2)} = x_c{}^{(1)}z_a{}^{(1)} + y_c{}^{(1)}z_b{}^{(1)} + z_c{}^{(1)2} - \frac{\partial(x^{(1)}, y^{(1)})}{\partial(a, b)}. \quad \text{(A4)}$$

REFERENCES

Aas, E., and G. Berge, 1976: Irradiance observations in the Norwegian and Barents seas. Rep. No. 23, Institute for Geophysics, University of Oslo, 42 pp.

Brown, R. A., 1980: Longitudinal instabilities and secondary flows in the planetary boundary layer: A review. *Rev. Geophys. Space Phys.*, **18,** 683–697.

Buckley, J. R., T. Gammelsrød, A. Johannessen, O. M. Johannessen, and L. P. Røed, 1979: Upwelling: Oceanic structure at the ice edge of the Arctic ice pack in winter. *Science,* **203,** 165–167.

Gammelsrød, T. A., M. Mork, and L. P. Røed, 1975: Upwelling possibilities at an ice edge, homogeneous model. *Mar. Sci. Commun.*, **1,** 115–145.

Gjevik, B., E. Nøst, and T. Straume, 1990: *Atlas of the Tides on the Shelves of the Norwegian and Barents Seas.* Department of Mathematics, University of Oslo, 74 pp.

Lamb, H., 1932: *Hydrodynamics,* 6th ed. Cambridge University Press. 738 pp.

Leibovich, S., 1983: The form and dynamics of Langmuir circulations. *Ann. Rev. Fluid Mech.*, **15,** 391–427.

Liu, A. K., and E. Mollo-Christensen, 1988: Wave propagation in a solid ice pack. *J. Phys. Oceanogr.*, **18,** 1702–1712.

Longuet-Higgins, M. S., 1953: Mass transport in water waves. *Phil. Trans. R. Soc. London,* **A 245,** 535–581.

——, 1962: The directional spectrum of ocean waves, and processes of wave generation. *Proc. R. Soc. London,* **A 265,** 286–315.

Lunde, T., 1963: Sea Ice in the Svalbard region 1957–1962. Norsk Polarinstitutt Årbok, 24–34.

Mosby, H., 1938: Svalbard waters. *Geofys. Publ.*, **12**(4), 85 pp.

Pierson, W. J., 1962: Perturbation analysis of the Navier-Stokes equations in Lagrangian form with selected linear solutions. *J. Geophys. Res.*, **67,** 3151–3160.

Pollard, R. T., 1970: Surface waves with rotation: An exact solution. *J. Geophys. Res.*, **75,** 5895–5898.

Røed, L. P., and J. J. O'Brien, 1983: A coupled ice–ocean model of upwelling in the marginal ice zone. *J. Geophys. Res.*, **88,** 2863–2872.

Squire, V. A., 1984: Sea ice. *Sci. Prog. Oxford,* **69,** 19–43.

——, and S. C. Moore, 1980: Direct measurement of the attenuation of ocean waves by pack-ice. *Nature,* **284,** 365–368.

Stokes, G. G., 1847: On the theory of oscillatory waves. *Trans. Cambridge Philos. Soc.*, **8,** 441–455.

Tabata, T., 1958: Studies on visco-elastic properties of sea ice. *Arctic Sea Ice,* Arctic Sea Ice Conf., Office of Naval Research, Easton, MD, 271 pp.

Wadhams, P., 1973: Attenuation of swell by sea ice. *J. Geophys. Res.*, **78,** 3552–3563.

——, and V. A. Squire, J. A. Ewing, and R. W. Pascal, 1986: The effect of the marginal ice zone on the directional wave spectrum of the ocean. *J. Phys. Oceanogr.*, **16,** 358–376.

Weber, J. E., 1983: Steady wind- and wave-induced currents in the open ocean. *J. Phys. Oceanogr.*, **13,** 524–530.

——, 1985: Friction induced roll motion in short-crested surface gravity waves. *J. Phys. Oceanogr.*, **15,** 936–942.

——, 1987: Wave attenuation and wave drift in the marginal ice zone. *J. Phys. Oceanogr.*, **17,** 2351–2361.

Woodcock, A. H., 1944: A theory of surface water motion deduced from the wind induced motion of the Physalia. *J. Mar. Res.*, **5**(3), 196–206.